Proceedings of ISSS-7, 26-31, March, 2005

Magnetospheric Sounding by IMAGE

James L. Green
Sciences and Exploration Directorate
NASA Goddard Space Flight Center, Greenbelt MD 20771 U.S.A.

The Radio Plasma Imager (RPI) on the Imager for Magnetopause-to-Aurora Global Exploration (IMAGE) spacecraft was designed as a long-range magnetospheric radio sounder, relaxation sounder, and a passive plasma wave instrument. The RPI is a highly flexible instrument that can be programmed to perform these types of measurements at times when IMAGE is located in key regions of the magnetosphere. The echoes observed by RPI are analyzed to obtain electron densities profiles all along the sounder ray paths allowing a comprehensive picture of the structure and dynamics of the inner magnetosphere to be created.

1. Introduction

The IMAGE spacecraft was launched on March 25, 2000 into a highly elliptical polar orbit with initial geocentric apogee of 8.22 Earth radii (R_E) and perigee altitude of 1000 km. The RPI instrument transmits coded electromagnetic waves over a selectable frequency range from 3 kHz to 3 MHz from a long dipole antenna. RPI utilizes three orthogonal dipole antennas of 325 m (X-axis), 500 m (Y-axis), and 20 m (Z-axis). The X-axis dipole is used for transmission while all antennas are used for the reception of the return echoes and for making passive radio measurements. For more details on the RPI instrument, see *Reinisch et al.* [2000]. The far-field radiation pattern of the RPI transmissions cover nearly all directions. From a sweep over a series of sounding frequencies RPI observes a wide variety of magnetospheric echoes. This short paper provides a brief overview of the type of RPI echoes observed and some of the results from their analysis.

2. Types of Echoes Observed

Figure 1A is an RPI plasmagram (signal strength as a function of virtual range and frequency) when the IMAGE spacecraft was just inside the plasmasphere. The virtual range is given by ct/2 where c is the free-space speed of light and t is the echo delay time. The echo intensity is color-coded. Three basic types of RPI echoes (field-aligned, diffuse, and resonance) are shown in Figure 1A.

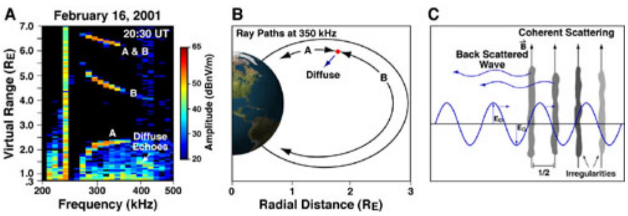

Fig 1. RPI plasmagram with field-aligned and diffuse echoes labeled (panel A). The directions of the observed echoes relative to the spacecraft position (panel B). The diffuse echoes are spread in range and are therefore reflecting from a series of irregularities (panel C).

Figure 1B shows the directions of the observed echoes relative to the spacecraft position. The diffuse echoes typically show range or frequency spreading whereas field-aligned (guided) echoes tend to appear as discrete traces in plasmagrams and often in multiple traces over the same frequency range. The diffuse resonances are spread in range due to reflections from a series of irregularities as shown in panel C. Plasma resonances observed by RPI appear as vertical emissions in plasmagrams (see section 7).

3. Diffuse Echoes

Based on direction analysis and the observed virtual ranges for the spacecraft observation location, the ray paths of the diffuse and field-aligned echoes of Figure 1A are shown schematically in Figure 1B. *Carpenter et al*. [2002] and *Fung et al.* [2003] attributed the range spreading of the diffuse echoes to coherent (aspect-sensitive) scattering from field-aligned electron density (N_e) irregularities (*FAI*) having < 10% variations of the background N_e that range in size from 200 m to a few km as illustrated in Figure 1C. *Carpenter et al.* [2002] also pointed out the possibility of refraction into and partial propagation along ducts having cross-field scales of several signal wavelengths.

4. Field-Aligned Echoes

From ray tracing calculations, *Fung and Green* [2005] have demonstrated that multiple traces of RPI discrete echoes of the type shown in Figure 1A are most likely due to ducted signals from conjugate hemispheres along closed field-aligned paths, analogous to the mechanism generally invoked to explain similar ionospheric observations. Figure 2 shows that ducting of nearly field-aligned propagating waves ($\psi \sim 0°$) occurring within N_e depletions as small as 1% and less than 10 wavelengths wide. Conjugate field-aligned echoes observed by RPI are most likely due to waveguide ducting with relatively smooth ducts, maintained along the plasmaspheric field lines.

In the case of ducting, *FAI* can act like a waveguide that traps and channels wave energy along the background magnetic field. For high-frequency electromagnetic waves ($f >> f_{uhr}$, where f_{uhr} is the upper hybrid resonance frequency), a region of N_e depletion extending some distance along the magnetic field may be able to trap wave energy by total internal reflections along a field-aligned N_e duct. The questions of generation and maintenance of field-aligned N_e ducts remain outstanding and require further investigation.

Echoes at different frequencies that propagate in the same mode and direction form a distinct trace on a plasmagram. Figure 3A shows five such traces; indicating that only a limited number of modes and propagation directions can produce strong echo traces. The five traces in Figure 3A were actually produced by three modes, labeled X and Z in the figure (the Z involves coupling to the O mode), each propagating parallel (toward the northern hemisphere, labeled N) and anti-parallel (toward the southern hemisphere, labeled S) to the magnetic field direction [*Reinisch et al.*, 2001].

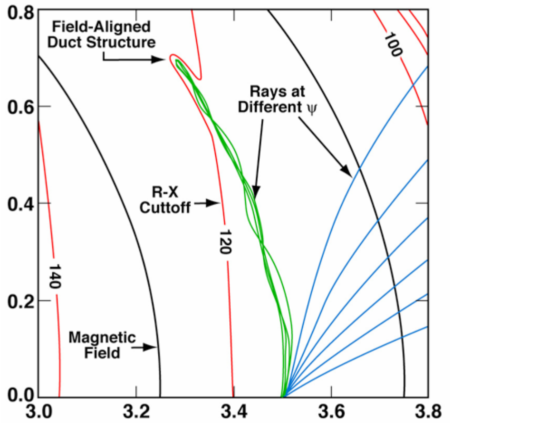

Fig. 2. Ray tracing calculations in a plasmaspheric density duct of free escaping R-X mode waves at 120 kHz. Rays launched within a few degrees of the magnetic field are ducted while other are refracted away.

The field-aligned N_e profiles in the two hemispheres, derived from the echo inversion technique are shown in Figure 3B as one curve, as a function of latitude. Multiple field-aligned N_e profiles obtained successively along the spacecraft track by RPI can be combined to produce a 2-dimensional N_e distribution along the field and along the IMAGE spacecraft track [*Huang et al.*, 2004]. When the spacecraft revisits the same region periodically in different orbits, plasma depletion and refilling and other dynamic processes can be investigated [*Reinisch et al.*, 2004].

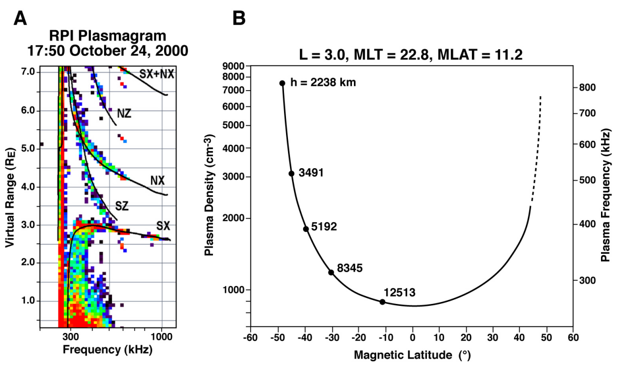

Fig. 3. The RPI plasmagram (panel A) shows field-aligned echoes, which allow inversion of the data into a field-aligned plasma electron density profile (panel B).

5. Plasmasphere Refilling

The time it takes for the plasmasphere to refill after the March 31, 2001 storm period can be determined by comparing those field-aligned N_e profiles with the profiles obtained during a quiet day with very low Kp. The March 31, 2001 storm was so strong that the enhanced cross tail electric field reduced the L value of the plasmapause to about 2.3 thereby emptying plasmaspheric flux tubes all the way out to the pre-storm plasmapause at L = 5. Typical RPI observations of guided echoes after this very large geomagnetic storm are shown in Figure 4A (as an example of one out of a succession of plasmagrams). Inverting the guided echoes gives a N_e profile shown in Figure 4B. The N_e along the same L value from the quiet day empirical model is also shown.

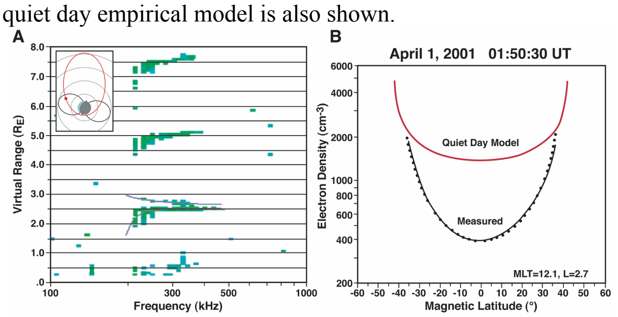

Fig. 4. Panel B compares the results of the inversion of the measured ducted echoes in panel A with the quiet day model of the plasmasphere. The quiet day model was constructed from observed ducted echoes during a time of low Kp.

A large difference in N_e is found in this comparison indicating the extensive loss of plasma that occurred during the geomagnetic storm period. Since plasmasphere filling is a process that can take a day or more, successive IMAGE passes through the plasmasphere can be used to monitor the filling process. The IMAGE/EUV observations clearly shows that the plasmasphere was stripped of cold plasma down to very low L values at all local times during this geomagnetic storm. A plasma convection tail was also observed by EUV in the late evening local time sector; however, the RPI observations were made along the orbit plane, which was primarily in the noon-midnight meridian avoiding any region of enhanced plasmaspheric material that would adversely effect the determination of the filling rate.

Figure 5 shows the RPI derived equatorial N_e normalized by the quiet day equatorial N_e from four consecutive passes of IMAGE through the plasmasphere. Since the IMAGE orbital period is approximately 14 hours, "snapshots" of plasmaspheric filling can be obtained every 14 hours. The inner plasmasphere, below about L of 2.3, shows no depletion from the storm while the equatorial densities at higher L values undergo extensive depletion. The refilling process at L = 2.8 started at approximately 1600 UT on April 1 and, as shown in Figure 5, is complete by about 2000 UT on April 2. The refilling of plasma in the plasmasphere at an L value of 2.8 is therefore completed in less than about 28 hours. These observations are consistent with those of *Park* [1974], who determined refilling times from whistler observations.

The RPI observations of guided echoes also provide a unique capability to compare RPI derived field-line N_e distributions with plasmasphere transport models. Comparisons by *Tu et al.,*

[2003] of RPI derived field-line N_e distributions with the field-line inter-hemispheric plasma (FLIP) model shows good agreement only for the equatorial region and that higher densities are found at higher latitudes. The agreement can be improved by invoking direct heating of ions in the plasmasphere at the equator during the time of plasmasphere refilling. Ion heating at the equator, and therefore enhanced ion pressure, will impede ionospheric flow into the equator giving rise to an increase in the N_e gradient along at the mid-latitudes.

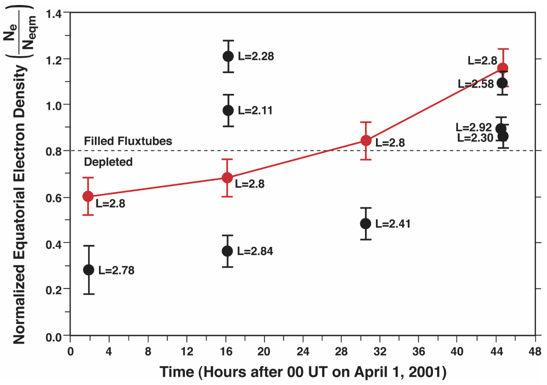

Fig. 5. A plot of the N_e at the equator normalized to the quiet day model as measured by RPI from four passes through the plasmasphere at a number of L shells. The curve at an L of 2.8 illustrates that this flux tube took approximately 28 hours to fill.

6. Polar Cap Electron Densities

During IMAGE apogee passages over the northern polar region, polar cap echo traces have been observed to last up to three hours [*Nsumei et al.,*2003]. In this high latitude region, the geomagnetic field lines are nearly radial, so that direct echoes from the polar cap and field-aligned guided echoes are not easily distinguishable. Inversion of polar cap traces (either from direct or guided echoes) will yield the nearly radial N_e profiles of the polar cap. *Nsumei et al*. [2003] created an empirical model as a function of K_p by appropriately binning and averaging the RPI N_e data. The result of this analysis is shown in Figure 6 along with a comparison of the *Persoon et al*. [1983] and *Gallagher et al*. [2000] polar cap models.

The Persoon, Gallagher, and Nsumei K_p =1 models agree relatively well. However, the RPI polar cap model clearly shows the dependence of the polar cap densities with increasing geomagnetic index K_p. The analysis in the Persoon and Gallagher models primarily involve interpretation of wave propagation cutoffs and particle measurements under low densities and spacecraft charging conditions, all of which typically underestimates polar cap N_e. The RPI echo observations have no such limitations and provide a much more realistic determination of the polar cap densities.

It is important to note that the RPI measurements were taken near solar maximum while the Persoon and Gallagher models were derived from observations that range over the entire solar cycle. This may account for some of the difference in the models. RPI's ability to obtain the polar cap N_e structure during individual passes will shed new light on the processes that governs polar wind outflow and the contributions of plasmas from auroral or polar cusp sources under different geomagnetic conditions. These studies are underway.

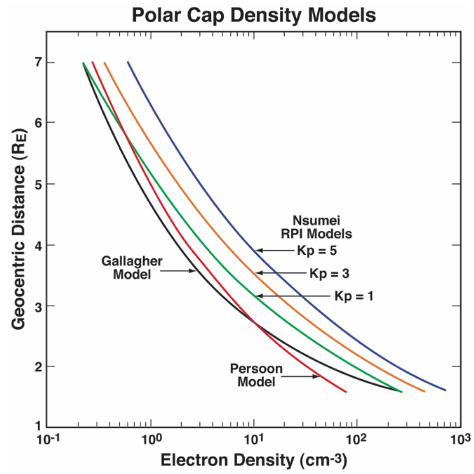

Fig. 6. RPI polar cap density models for three separate K_p ranges derived from 108 plasmagrams. The average polar cap densities for low K_p compares reasonably well with the previously published model results of Gallagher and Persoon, however, the RPI model densities for large K_p indices are significantly higher (by a factor of ~10).

7. Local Sounding

The RPI is also a relaxation sounder that generates and detects short-range electrostatic wave echoes at the various resonance frequencies or normal modes of a plasma. Like many other missions that have preceded IMAGE (e.g. GEOS 1, ISEE 1) a relaxation-sounder permits accurate determination of the local N_e and magnitude of the magnetic field (**B**) at the spacecraft when the resonances have been properly identified. The advantage of the RPI over other magnetospheric relaxation sounders is that it has enough power to generate the long-range electromagnetic echoes (as described in the previous sections) that can uniquely identify the X and O mode local cutoff frequencies and thereby allow for the proper identification of all the natural plasma resonances observed.

The local N_e and **B** are determined mainly from the measured frequencies of the sounder-stimulated plasma resonances at f_p, f_g, and nf_g (where n = 2, 3, and larger values). Other resonances, such as the Q and D resonances, can also be used to determine these parameters but only when care is taken to properly identify the resonances at frequencies both above the upper hybrid resonance frequency (f_{uhr}) and below the plasma frequency. Use of the resonance measurements can allow for the determination of the f_p to within ~1% and f_g to within ~0.1%.

Figure 7 shows two plasmagrams with plasma resonances taken near apogee one orbit apart just before (panel A) and during (panel B) a geomagnetic storm using the Z axis antenna. Figure 7 is the result of an extensive resonance analysis process that begins by resorting the RPI data with respect to the gyrofrequency harmonics (see *Benson, et al*., 2003 for more details on this technique). Since all the Q and D resonances have a gyrofrequency dependency then they too can be identified in this new coordinate system. D resonances appear below the plasma frequency (f_p) and Q resonances appear above the plasma frequency. The resulting identified resonances are then plotted onto the plasmagram to create Figure 7.

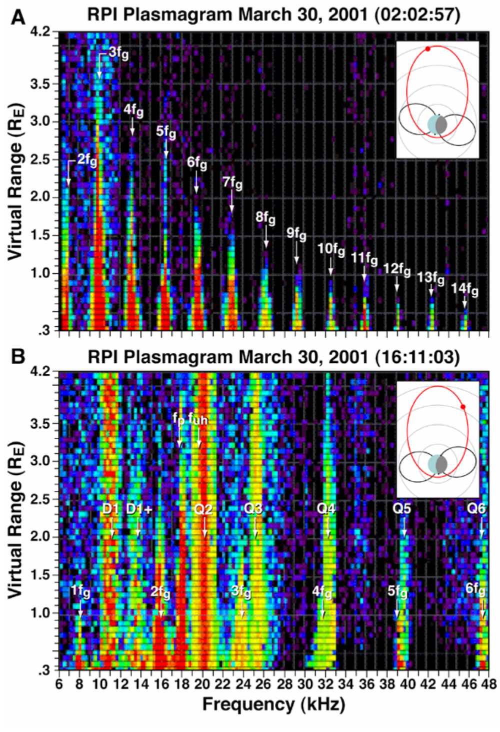

Fig. 7. Two RPI plasmagrams showing the local plasma resonances conditions near apogee on consecutive orbits prior (panel A) and during (panel B) a large geomagnetic storm.

The only resonances measured in Figure 7A are from the harmonics of the gyrofrequencies (f_g) whose value has been determined to be 2.375 kHz. The local f_p must be below 6 kHz since that is the frequency at the start of the sounding sequence. The observed resonances in Figure 7B, one orbit later, are significantly different and show f_p, nf_g, Q, and D resonances. These storm time observations show that f_g is now over 8 kHz and the observed f_p is ~17.4 kHz. The observed Q resonances, or Bernstein mode waves, have group velocities nearly matched to the spacecraft, and have been observed in the ionosphere and magnetosphere [*Benson et al.*, 2003] at frequencies between the f_g harmonics and above f_{uhr}. Prior to the launch of IMAGE, the D resonances had only been reported in the topside ionosphere at frequencies between the f_g harmonics and below f_{uhr}. There has been an on-going controversy as to the existence in planetary magnetosphere of the D resonances but it is now clear from the RPI resonance observations that these D resonances are similar to those stimulated by topside sounders in spite of the large differences in the electron temperatures. In light of the intense D resonances easily observed by RPI, previously published results from other magnetospheric relaxation sounders may need to be re-examined for the D resonances.

8. Conclusions

The long-range sounder echoes from RPI allow remote sensing of a variety of plasmas structures and boundaries in the magnetosphere. A profile inversion technique for RPI echo traces has been developed and provides a method for determining the N_e distribution of the plasma from either direct or field-aligned echoes. This technique has enabled the determination of the evolving N_e structure of the polar cap and the plasmasphere under a variety of geomagnetic conditions.

Acknowledgments I would like to gratefully acknowledge the University of Massachusetts group headed by Prof. Bodo Reinisch who pioneered the RPI instrument and much of the data analysis software. This research was support by NASA under SECGIP03-0085.

References

Benson, R. F., et al., Classification of IMAGE/RPI-stimulated plasma resonances for the accurate determination of magnetospheric electron-density and magnetic field values, *J. Geophys. Res.*, **108**(A5), 1207, doi:10.1029/2002JA 009589, 2003.

Carpenter, D. L., et al., Small-scale field-aligned plasmaspheric density structures inferred from RPI on IMAGE, *J. Geophys. Res.*, **107**(A9), 1258, 10.1029/2001JA009199, 2002.

Fung, S. F., et al., Guided Echoes in the Magnetosphere: Observations by Radio Plasma Imager on IMAGE, *Geophys. Res. Lett.*, **30**(11), 1589, doi:10.1029/2002GL016531, 2003.

Fung, S. F. and J. L., Green, Modeling of field-aligned radio echoes in the plasmasphere, *J. Geophys. Res.*, **110**, A01210, doi:10.1029/2004 JA010658, 2005.

Gallagher, D. L., P. D. Craven, and R. H. Comfort, Global core plasma model, *J. Geophys. Res.*, **105**, 18819, 2000.

Huang, X., et al., Developing an empirical model of the plasmasphere using IMAGE/RPI data, *Adv. Space Res.*, **33** (6), 829-832, 2004.

Nsumei, P. A., et al., Electron density distribution over the northern polar region deduced from IMAGE/RPI sounding, *J. Geophys. Res.*, **108**(A2), 10.1029/2002JA009616, 2003.

Park, C. G., Some features of plasma distribution in the plasmasphere deduced from Antarctic whistlers, , *J. Geophys. Res.*, **79**, 169, 1974.

Persoon, A. M., et al., Polar cap electron densities from DE 1 plasma wave observations, *J. Geophys. Res.*, **88**, 10123, 1983.

Reinisch, B. W., et al., The Radio Plasma Imager investigation on the IMAGE spacecraft, *Space Science Reviews*, **91**, 319-359, 2000.

Reinisch, B.W., et al., Plasma Density Distribution Along the Magnetospheric Field: RPI Observations from IMAGE, *Geophys. Res. Lett.*, **28**, 24, 4521-4524, 2001.

Reinisch, B. W., et al., Plasmaspheric mass loss and refilling as a result of a magnetostorm,*J.Geophys.Res*.,doi:10.1029/2003JA09948, 2004.

Tu, J., et al., Simulating plasmaspheric field-aligned density profiles measured with IMAGE/RPI: Effects of plasmasphere refilling and ion heating, *J. Geophys. Res.*, doi:10.1029/2002JA009468, 2003.